

R. E. Saad, et. al.. "Tactile Sensing."

Copyright 2000 CRC Press LLC. <<http://www.engnetbase.com>>.

Tactile Sensing

R. E. Saad

University of Toronto

A. Bonen

University of Toronto

K. C. Smith

University of Toronto

B. Benhabib

University of Toronto

- 25.1 Sensing Classification
- 25.2 Mechanical Effects of Contact
Simplified Theory for Tactile Sensing • Requirements for
Tactile Sensors
- 25.3 Technologies for Tactile Sensing
Resistive • Capacitive • Piezoelectric • Optical • Photoelastic

Robots in industrial settings perform repetitive tasks, such as machine loading, parts assembly, painting, and welding. Only in rare instances can these autonomous manipulators modify their actions based on sensory information. Although, thus far, a vast majority of research work in the area of robot sensing has concentrated on computer vision, contact sensing is an equally important feature for robots and has received some attention as well. Without tactile-perception capability, a robot cannot be expected to effectively grasp objects. In this context, robotic tactile sensing is the focus of this chapter.

25.1 Sensing Classification

Robotic sensing can be classified as either of the noncontact or contact type [1]. *Noncontact sensing* involves interaction between the robot and its environment by some physical phenomenon, such as acoustic or electromagnetic waves, that interact without contact. The most important types of robotic sensors of the noncontact type are vision and proximity sensors. *Contact sensing*, on the other hand, implies measurement of the general interaction that takes place when the robot's end effector is brought into contact with an object. Contact sensing is further classified into force and tactile sensing.

Force sensing is defined as the measurement of the global mechanical effects of contact, while *tactile sensing* implies the detection of a wide range of local parameters affected by contact. Most significant among those contact-based effects are contact stresses, slippage, heat transfer, and hardness.

The properties of a grasped object that can be derived from tactile sensing can be classified into geometric and dynamometric types [2]. Among the geometric properties are presence, location in relation to the end-effector, shape and dimensions, and surface conditions [3–7]. Among the dynamometric parameters associated with grasping are: force distribution, slippage, elasticity and hardness, and friction [8–12].

Tactile sensing requires sophisticated transducers; yet the availability of these transducers alone is not a sufficient condition for successful tactile sensing. It is also necessary to accurately control the modalities through which the tactile sensor interacts with the explored objects (including contact forces, as well as end-effector position and orientation) [13–15]. This leads to active tactile sensing, which requires a high degree of complexity in the acquisition and processing of the tactile data [16].

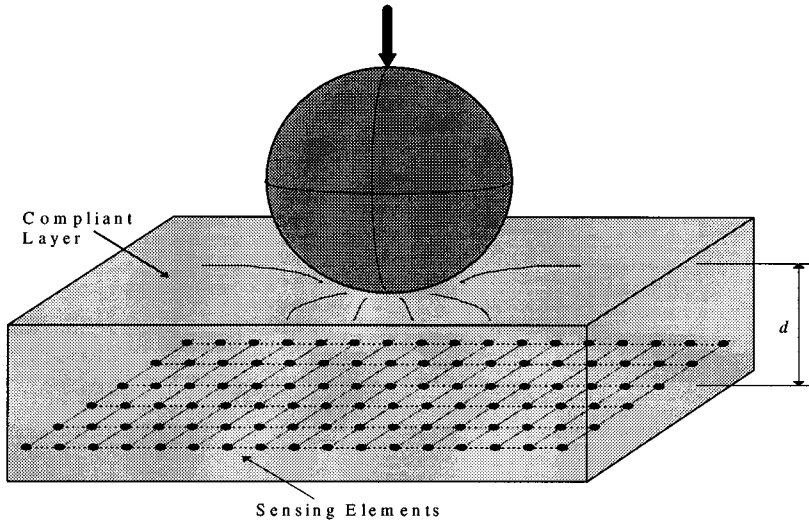


FIGURE 25.1 An object indenting a compliant layer, where an array of force-sensing elements is placed at a distance d from the surface.

25.2 Mechanical Effects of Contact

Tactile sensing normally involves a rigid object indenting the compliant cover layer of a tactile sensor array [17], [Figure 25.1](#). The indentation of a compliant layer due to contact can be analyzed from two conceptually different points of view [1]. The first one is the measurement of the actual contact stresses (force distribution) in the layer, which is usually relevant to controlling manipulation tasks. The second one is the deflection profile of the layer, which is usually important for recognizing geometrical object features. Depending on the approach adopted, different processing and control algorithms must be utilized.

There exists a definite relationship between the local shape of a contacting body and a set of subsurface strains (or displacements); however, this relationship is quite complex. Thus, it requires the use of the Theory of Elasticity and Contact Mechanics to model sensor–object interaction [18], and the use of Finite Element Analysis (FEA) as a practical tool for obtaining a more representative model of the sensor [19].

In general, the study of tactile sensors comprises two steps: (1) the *forward analysis*, related to the acquisition of data from the sensor (changes on the stress or strains, induced by the indentation of an object on the compliant surface of the transducer); and, (2) the *inverse problem*, normally related to the recovery of force distribution or, in some cases, the recovery of the indenter's shape.

Simplified Theory for Tactile Sensing

For simplicity, the general two-dimensional tactile problem is reduced herein to a one-dimensional one. [Figure 25.2](#) shows a one-dimensional transducer that consists of a compliant, homogeneous, isotropic, and linear layer subjected to a normal stress $q_v(x)$ created by the indentation of an object.

For modeling purposes, it is assumed that the compliant layer is an elastic half-space. This simplification yields closed-form equations for the analysis and avoids the formation of a more complex problem, in which the effect of the boundary conditions at x_{\min} and x_{\max} must be taken into account. It has been proven that the modeling of the sensor by an elastic half-space represents a reasonable approximation to the real case [18]. Under these conditions, it can be shown that the normal strain, at a depth $y = d$, due to the normal stress $q_v(y)$ is given by [20]:

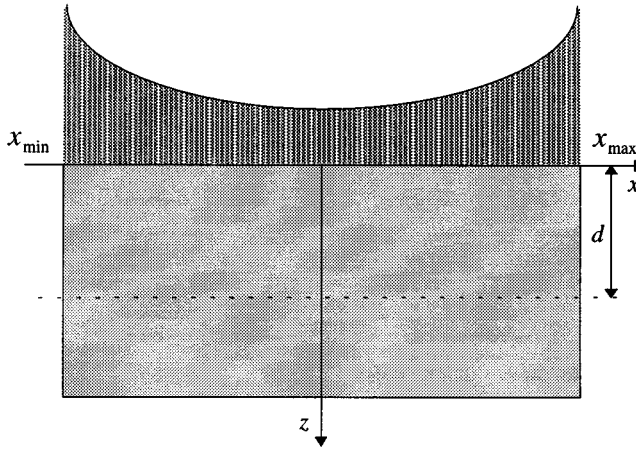


FIGURE 25.2 Ideal one-dimensional transducer subjected to a normal stress.

$$\epsilon_z(x) = \int_{-\infty}^{\infty} q_v(x-x_0)h_z(x_0,d) dx_0 \quad (25.1)$$

where ϵ_z is the strain at x and $z = d$ due to the normal stress on the surface, and

$$h_z(x) = -\frac{2d(1+\nu)[d^2(1-\nu)-vx^2]}{\pi rE(x^2+d^2)^2} \quad (25.2)$$

E and ν are, respectively, the modulus of elasticity and the Poisson's coefficient of the compliant layer. In obtaining Equation 25.2, it is assumed that the analysis is performed under *planar strain* conditions. It should be noted that a similar analysis can be performed for tangential contact stresses or strains.

The normal displacement at the surface, w , is given by:

$$w(x) = \int_{-\infty}^{\infty} q_v(x-x_0)k(x_0) dx_0 \quad (25.3)$$

where

$$k(x) = \frac{-2(1-\nu^2)}{\pi E} \log \left| \frac{x}{x_a} \right| \quad (25.4)$$

The singularity at $x = 0$ is expected due to the singularity of stress at that point. Note that, $k(x)$ is the deformation of the surface when a singular load of 1 N is applied at $x = 0$. The constant x_a should be chosen such that at $x = x_a$, the deformation is zero. In this case, zero deformation should occur at $x \rightarrow \infty$ (note that it has been assumed that the sensor is modeled by an elastic half space), namely $x_a \rightarrow \infty$. This problem is associated with the two-dimensional deformation of an elastic half-space. To eliminate this difficulty, the boundary conditions of the transducer must be taken into account (i.e., a finite transducer must be analyzed), which requires, in general, the use of FEA.

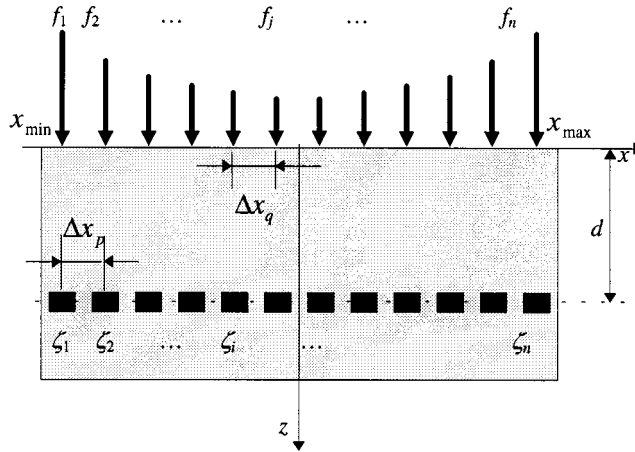


FIGURE 25.3 One-dimensional transducer with discrete sensing elements located at $z = d$.

Since measurements of strain (or stress) are usually done by a discrete number of sensing elements, Equation 25.2 must be discretized (Figure 25.3). Correspondingly, the force distribution must be reconstructed at discrete positions as shown in Figure 25.3. Let Δx_q be the distance between points, where the force distribution must be reconstructed from strain (or stress) measurements carried out by strain (or stress) sensing elements uniformly distributed at intervals Δx_p , at $z = d$. Also assume, even though it is not necessary, that $\Delta x_q = \Delta x_p = \Delta x$ and that the forces are applied at positions immediately above the sensor elements. One can now define the strain (stress)-sample vector, ζ , whose components are given by $\zeta_i = \epsilon_x(x_i)$, $i = 1, 2, \dots, n$, and the force distribution vector, F whose components are given by $f_j = q_v(x_j)$, $j = 1, 2, \dots, n$. Then, the discrete form of Equation 25.1 is given by:

$$\zeta = \mathbf{T}F \quad (25.5)$$

where the elements of the matrix \mathbf{T} are given by $T_{ij} = k_v(x_i - x_j)$, $i = 1, 2, \dots, n$ and $j = 1, 2, \dots, n$ [23]. A similar relation to Equation 25.5 can be obtained discretizing Equation 25.3. In the general case, where $\Delta x_q \neq \Delta x_p$, \mathbf{T} is not square. Furthermore, in the general case, the vector F comprises both vertical and tangential components.

Equations 25.1 and 25.3 represent the regular *forward problem*, while Equation 25.5 represents the discretized version of the forward problem. The *inverse problem*, in most cases, consists of recovering the applied force profile from the measurements of strain, stress, or deflection. (Note that the surface displacement can also be used to recover the indenter's shape.)

In [20], it was shown that the inverse problem is ill-posed because the operators h and k , of Equations 25.1 and 25.3, respectively, are ill-conditioned. Consequently, the inverse problem is susceptible to noise. To solve this problem, regularization techniques must be utilized [20].

It has been proven that, in order to avoid aliasing in determining the continuous strain (stress) at a depth d using a discretized transducer, the elements have to be separated by one tenth of the compliant layer's thickness. However, good results were obtained, without much aliasing, by separating the sensing elements by a distance equal to the sensor's depth [18].

Requirements for Tactile Sensors

In 1980, Harmon conducted a survey to determine general specifications for tactile sensors [21]. Those specifications have been used subsequently as guidelines by many tactile sensor designers:

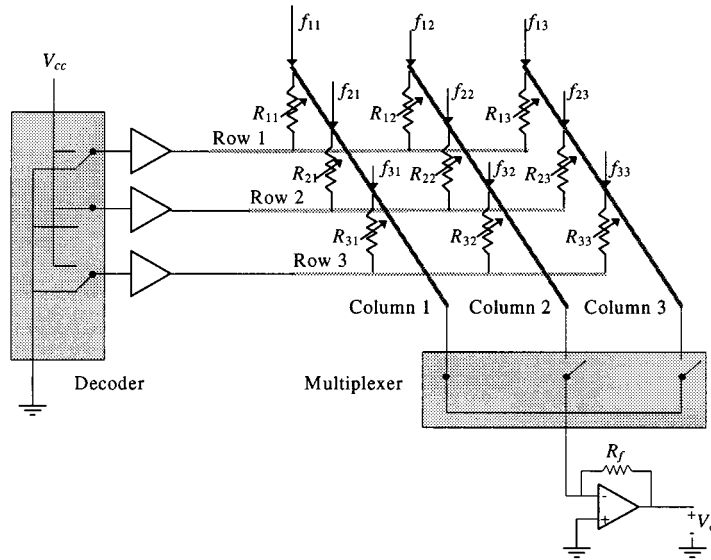


FIGURE 25.4 General configuration of a resistive transducer.

1. Spatial resolution of 1 to 2 mm
2. Array sizes of 5×10 to 10×20 points
3. Sensitivity of 0.5×10^{-2} to 1×10^{-2} N for each force-sensing element (tactel)
4. Dynamic range of 1000:1
5. Stable behavior and with no hysteresis
6. Sampling rate of 100 Hz to 1 kHz
7. Monotonic response, though not necessarily linear
8. Compliant interface, rugged and inexpensive

While properties (5), (7), and (8) above should apply to any practical sensor, the others are merely suggestions, particularly with respect to the number of array elements and spatial resolution.

Developments on tactile sensing following [21] have identified additional desirable qualities; namely, reliability, modularity, speed, and the availability of multisensor support [16].

25.3 Technologies for Tactile Sensing

The technologies associated with tactile sensing are quite diverse: extensive surveys of the state-of-the-art of robotic-tactile-transduction technologies have been presented in [2, 3, 16, 17]. Some of these technologies will be briefly discussed.

Resistive

The transduction method that has received the most attention in tactile sensor design is concerned with the change in resistance of a conductive material under applied pressure. A basic configuration of a resistive transducer is shown in Figure 25.4. Each resistor, whose value changes with the magnitude of the force, represents a resistive cell of the transducer. Different materials have been utilized to manufacture the basic cell.

Conductive elastomers were among the first resistive materials used for the development of tactile sensors. They are insulating, natural or silicone-based rubbers made conductive by adding particles of conductive or semiconductive materials (e.g., silver or carbon). The changes in resistivity of the elastomers

under pressure are produced basically by two different physical mechanisms. In the first approach, the change in resistivity of the elastomer under pressure is associated with deformation that alters the particle density within it. Two typical designs of this kind are given in [22, 23]. In the second approach, while the bulk resistance of the elastomer changes slightly when it is compressed, the design allows the increase of the area of contact between the elastomer and an electrode, and correspondingly a change in the contact resistance. A typical design of this kind is given in [24]. In [25], a newer tactile sensor is reported with both three-axis force sensing and slippage sensing functions. In the former case, the pressure sensing function is achieved utilizing arrays of pressure transducers that measure a change in contact resistance between a specially treated polyimide film and a resistive substrate.

Piezoresistive elements have also been used in several tactile sensors. This technology is specifically attractive at present because, with micromachining, the piezoresistive elements can be integrated together with the signal-processing circuits in a single chip [26]. A 32×32 -element silicon pressure sensor array incorporating CMOS processing circuits for the detection of a high-resolution pressure distribution was reported in [8]. The sensor array consists of an x–y-matrix-organized array of pressure cells with a cell spacing of $250 \mu\text{m}$. CMOS processing circuits are formed around the array on the same chip. Fabrication of the sensor array was carried out using a 3 mm CMOS process combined with silicon micromachining techniques. The associated diaphragm size is $50 \mu\text{m} \times 50 \mu\text{m}$. The overall sensor-array chip size is $10 \text{mm} \times 10 \text{mm}$.

In Figure 25.4, a circuit topology, to scan a 3×3 array of piezoresistive elements, is shown. The basic idea was originally proposed in [24] and adapted on several occasions by different researchers. Using this method, the changes in resistance are converted into voltages at the output. With the connections as shown in Figure 25.4, the resistance R_{21} can be determined from:

$$V_o = \frac{R_f}{R_{21}} V_{cc} \quad (25.6)$$

where V_o is the output voltage, V_{cc} is the bias voltage, and R_f is the feedback resistance of the output amplifier stage.

One problem with the configuration shown in Figure 25.4 is the difficulty in detecting small changes in resistance due to the internal resistance of the multiplexer as well changes in the voltage of power source, which have a great influence at the output. Other methods utilized to scan resistive transducer arrays are summarized in [3].

When piezoresistors and circuits are fabricated on the same silicon substrate, the sensor array can be equipped with a complex switching circuit, next to the sensing elements, that allows a better resolution in the measurements [9].

Capacitive

Tactile sensors within this category are concerned with measuring capacitance, which varies under applied load. The capacitance of a parallel-plate capacitor depends on the separation of the plates and their areas. A sensor using an elastomeric separator between the plates provides compliance such that the capacitance will vary according to the applied normal load, Figure 25.5(a).

Figure 25.5(b) shows the basic configuration of a capacitive tactile sensor. The intersections of rows and columns of conductor strips form capacitors. Each individual capacitance can be determined by measuring the corresponding output voltage at the selected row and column. To reduce cross-talk and electromagnetic interference, the rows and columns that are not connected are grounded. Figure 25.5(c) shows an equivalent circuit when the sensor is configured to measure the capacitance formed at the intersection of row i and row j , C_{ij} , R_d is the input resistance of the detector and C_d represents the effects of the stray capacitances, including the detector-amplifier input capacitance, the stray capacitance due

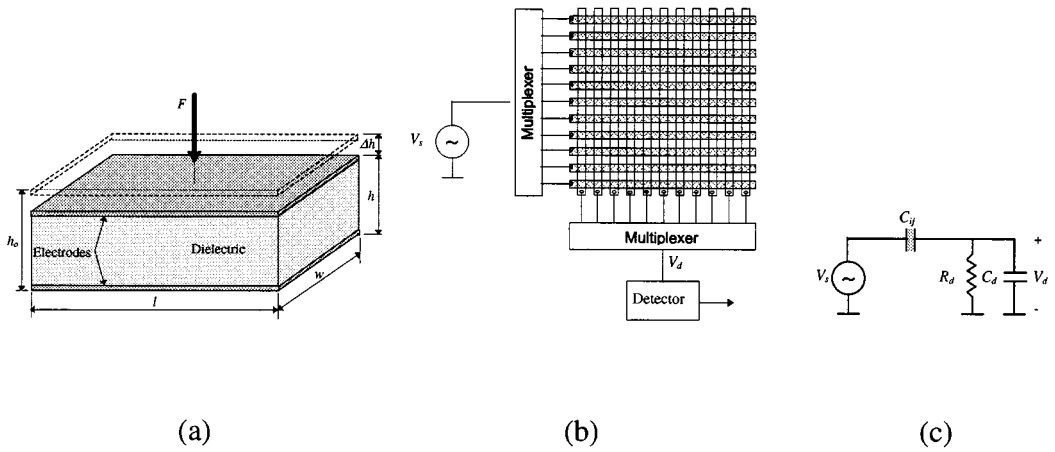


FIGURE 25.5 (a) Basic cell of a capacitor tactile sensor. (b) Typical configuration of a capacitive tactile sensor. (c) Equivalent circuit for the measurement of the capacitance C_{ij} .

to the unselected rows and columns, and the capacitance contributed by the cable that connects the transducer to the detector. Since the stray capacitance due to the unselected rows and columns changes with the applied forces, the stray capacitance due to the cable is designed to be predominant [18].

The magnitude of voltage at the input of the detector, $|V_d|$ is given by:

$$|V_d| = \frac{C_{ij} R_d \omega}{\sqrt{1 + [\omega R_d (C_{ij} + C_d)]^2}} |V_s| \quad (25.7)$$

Assuming that $C_d \gg C_{ij}$ and ω is sufficiently large,

$$|V_d| \cong \frac{C_{ij}}{C_d} |V_s| \quad (25.8)$$

When a load is applied to the transducer, the capacitor is deformed as shown in Figure 25.5(a). For modeling purposes, it is assumed that the plate capacitor is only under compression. When no load is applied, the capacitance due to the element in the i th row and the j th column, C_{ij}^0 , is given by:

$$C_{ij}^0 = \epsilon \frac{wl}{h_0} \quad (25.9)$$

where ϵ is the permittivity of the dielectric, w and l are the width and the length of the plate capacitor, respectively, and h_0 is the distance between plates when no load is applied. The voltage at the input of the detector for this particular case is indicated by V_{d0} ; then from Equation 25.8, one obtains:

$$|V_{d0}| \cong \frac{C_{ij}^0}{C_d} |V_s| \quad (25.10)$$

When a load is applied, the capacitor is under compression and the capacitance is given by:

$$C_{ij} = \epsilon \frac{wl}{h_0 - \Delta h} \quad (25.11)$$

The strain in this case is given by:

$$\zeta_z \cong \frac{\Delta h}{h_0} \quad (25.12)$$

where Δh is the displacement of the top metal plate and $\Delta h \ll h_0$. The strain can be measured by:

$$\frac{|V_d| - |V_{d0}|}{|V_d|} = \frac{\frac{C_{ij}}{C_d} - \frac{C_{ij}^0}{C_d}}{\frac{C_{ij}}{C_d}} = 1 - \frac{C_{ij}^0}{C_{ij}} = 1 - \frac{h_0 - \Delta h}{h_0} = \frac{\Delta h}{h_0} = \frac{\Delta h}{h_0} \cong \zeta_z \quad (25.13)$$

Consequently, the strain at each tactel can be determined by measuring the magnitudes of V_d and V_{d0} for each element.

Note that the presence of a tangential force would offset the plates tangentially and change the effective area of the capacitor plates. An ideal capacitive pressure sensor can quantify basic aspects of touch by sensing normal forces, and can detect slippage by measuring tangential forces. However, distinguishing between the two forces at the output of a single sensing element is a difficult task and requires a more complex transducer than the one presented in Figure 25.5(a) [27].

Micromachined, silicon-based capacitive devices are especially attractive due to their potential for high accuracy and low drift. A sensor with 1024 elements and a spatial resolution of 0.5 mm was reported in [28]. Several possible structures for implementing capacitive high-density tactile transducers in silicon have been reported in [29]. A cylindrical finger-shaped transducer was reported in [18].

The advantages of capacitive transducers include: wide dynamic range, linear response, and robustness. Their major disadvantages are susceptibility to noise, sensitivity to temperature, and the fact that capacitance decreases with physical size, ultimately limiting the spatial resolution. Research is progressing toward the development of electronic processing circuits for the measurement of small capacitances using charge amplifiers [30], and the development of new capacitive structures [29].

Piezoelectric

A material is called piezoelectric, if, when subjected to a stress or deformation, it produces electricity. Longitudinal piezoelectric effect occurs when the electricity is produced in the same direction of the stress, Figure 25.6. In Figure 25.6(a), a normal stress σ ($= F/A$) is applied along the Direction 3 and the charges are generated on the surfaces perpendicular to Direction 3. A transversal piezoelectric effect occurs when the electricity is produced in the direction perpendicular to the stress.

The voltage V generated across the electrodes by the stress σ is given by:

$$V = d_{33} \frac{h}{\epsilon} \sigma \quad (25.14)$$

where d_{33} = Piezoelectric constant associated with the longitudinal piezoelectric effect

ϵ = Permittivity

h = Thickness of the piezoelectric material

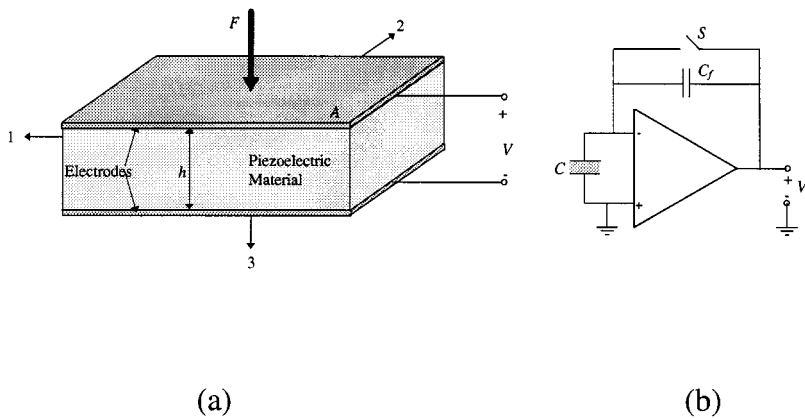


FIGURE 25.6 (a) Basic cell of a piezoelectric transducer. (b) Charge amplifier utilized for the measurement of the applied force.

Since piezoelectric materials are insulators, the transducer shown in Figure 25.6(a), can be considered as a capacitor, from an electrical point of view. Consequently,

$$V = \frac{Q}{C} = \frac{Q}{\epsilon A} h \quad (25.15)$$

where Q = Charge induced by the stress σ
 C = Capacitance of the parallel capacitor
 A = Area of each electrode

A comparison of Equations 25.14 and 25.15 leads to:

$$Q = d_{33} A \sigma \quad (25.16)$$

It is concluded that the force applied to the photoelastic material can be determined by finding the charge Q . Charge amplifiers are usually utilized for determining Q . The basic configuration of a charge amplifier is shown in Figure 25.6(b). The charge generated in the transducer is transferred to the capacitor C_f and the output voltage, V_o is given by:

$$V_o = -\frac{Q}{C_f} \quad (25.17)$$

The circuit must periodically discharge the feedback capacitor C_f to avoid saturation of the amplifier by stray charges generated by the offset voltages and currents of the operational amplifier. This is achieved by a switch as shown in Figure 25.6(b) or by a resistor parallel to C_f .

The piezoelectric material most widely used in the implementation of tactile transducers is PVF2. It shows the largest piezoelectric effect of any known material. Its flexibility, small size, sensitivity, and large electrical output offer many advantages for sensor applications in general, and tactile sensors in particular. Examples of tactile sensors implemented with this technology can be found in [1, 31].

The major advantages of the piezoelectric technology are its wide dynamic range and durability. Unfortunately, the response of available materials does not extend down to dc and therefore steady loads cannot be measured directly. Also, the PVF2 material produces a charge output that is prone to electrical interference and is temperature dependent.

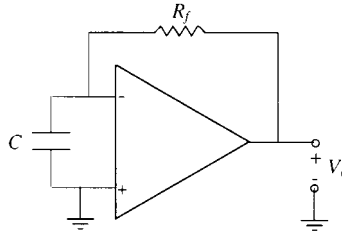


FIGURE 25.7 Current-to-voltage converter.

The possibility of measuring transient phenomenon using piezoelectric material has recently encouraged some researchers to use the piezoelectric effect for detecting vibrations that indicate incipient slip, occurrence of contact, local change in skin curvature, and estimating friction and hardness of the object [7, 10, 11]. If the piezoelectric transducer shown in Figure 25.6(a) is connected to an FET-input operational amplifier configured as a current-to-voltage converter as shown in Figure 25.7, the output voltage is given by:

$$V_o = \frac{dQ}{dt} R_f = AR_f d_{33} \frac{d\sigma}{dt} \quad (25.18)$$

where R_f is the feedback resistor. Correspondingly, the circuit configuration provides the mean to measure of changes in the contact stress. A detailed explanation of the behavior of this sensor can be found in [7].

Optical

Recent developments in fiber optic technology and solid-state cameras have led to numerous novel tactile sensor designs [32, 33]. Some of these designs employ flexible membranes incorporating a reflecting surface, Figure 25.8. Light is introduced into the sensor via a fiber optic cable. A wide cone of light propagates out of the fiber, reflects back from the membrane, and is collected by a second fiber. When an external force is applied onto the elastomer, it shortens the distance between the reflective side of the

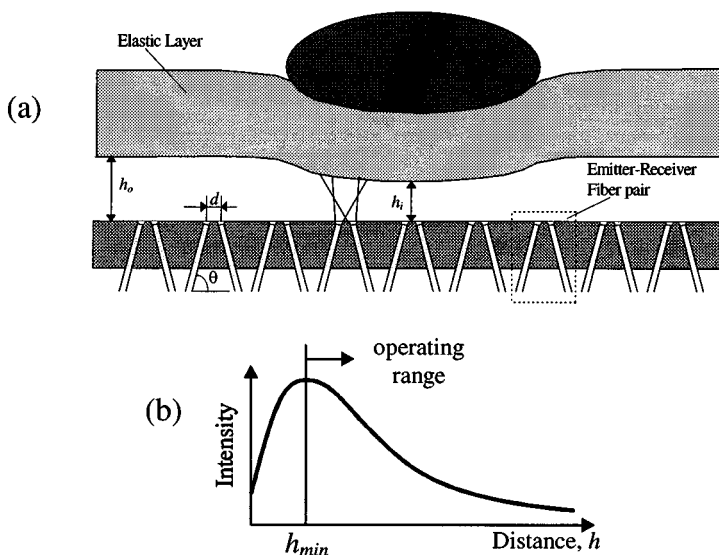


FIGURE 25.8 (a) Reflective transducer. (b) Light-intensity as a function of the distance h .

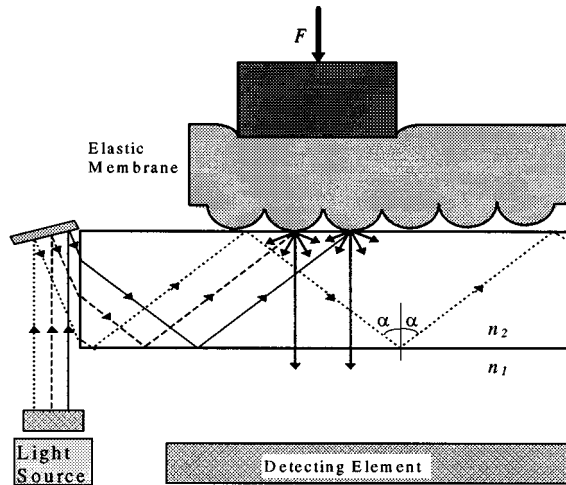


FIGURE 25.9 Tactile transducer based on the principle of internal reflection.

membrane and the fibers, h . Consequently, the light gathered by the receiving fiber changes as a function of h , Figure 25.8(b). To recover univocally the distance from the light intensity, a monotonic function is needed. This can be achieved by designing the transducer such it operates for $h > h_{\min}$, where h_{\min} is indicated in Figure 25.8(b). (The region $h > h_{\min}$ is preferred to the $h < h_{\min}$ for dynamic range reasons.)

Another optical effect that can be used is that of frustrated total internal reflection [5, 34]. With this technique, an elastic rubber membrane covers, without touching, a glass plate (waveguide); light entering the side edge of the glass is totally reflected by the top and bottom surfaces and propagates along it, Figure 25.9.

The condition for total internal reflection occurs when:

$$n_2 \sin \alpha \leq n_1 \quad (25.19)$$

where n_1 = Index of refraction of the medium surrounding the waveguide (in this case air, $n_1 \cong 1$)

n_2 = Index of refraction of the waveguide

α = Angle of incidence at the interface glass-air

Objects in contact with the elastic membrane deform it and induce contact between the bottom part of the membrane and the top surface of the waveguide, disrupting the total internal reflection. Consequently, the light in the waveguide is scattered at the contact location. Light that escapes through the bottom surface of the waveguide can be detected by an array of photodiodes, a solid-state sensor, or, alternatively, transported away from the transducer by fibers [3]. The detected imaged is stored in a computer for further analysis. A rubber membrane with a flat surface yields a high-resolution binary (contact or noncontact) image [5]. If the rubber sheet is molded with a textured surface (Figure 25.9), then an output proportional to the area of contact is obtained and, consequently, the applied forces can be detected [3]. Shear forces can also be detected using special designs [35]. Sensors based on frustrated internal reflection can be molded into a finger shape [5] and are capable of forming very high-resolution tactile images. Such sensors are commercially available. An improved miniaturized version of a similar sensor was proposed in [34].

Other types of optical transducers use “occluder” devices. One of the few commercially available tactile sensors uses this kind of transducer [36]. In one of the two available designs, the transducer’s surface is made of a compliant material, which has on its underside a grid of elongated pins. When force is applied to the compliant surface, the pins on the underside undergo a mechanical motion normal to the surface,

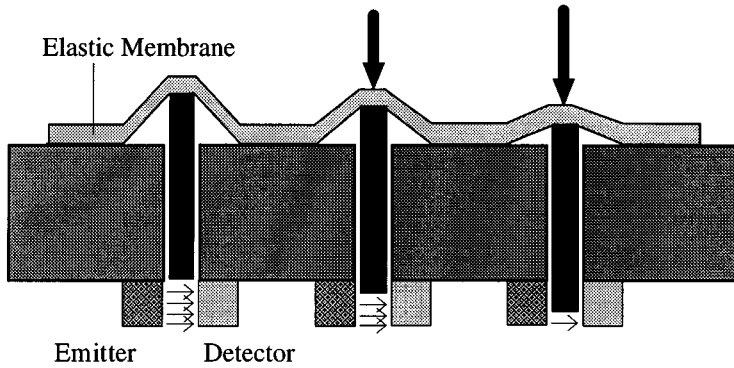


FIGURE 25.10 Principle of operation of an occluder transducer.

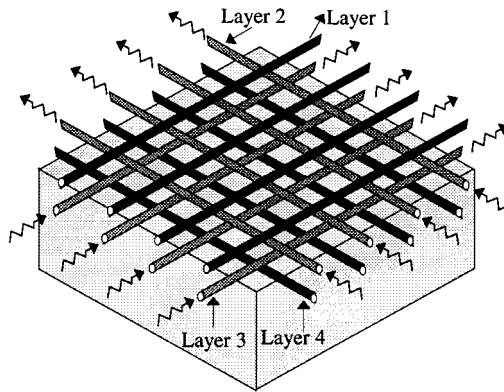


FIGURE 25.11 A four-layer tactile transducer.

blocking the light path of a photoemitter–detector pair. The amount of movement determines the amount of light reaching the photoreceiver. Correspondingly, the more force applied, the less amount of light is collected by the photoreceiver, [Figure 25.10](#). The major problems with this specific device are associated with creep, hysteresis, and temperature variation. This scheme also requires individual calibration of each photoemitter–photodetector pair.

Fibers have also been used directly as transducers in the design of tactile sensors. Their use is based on two properties of fiber optic cables: (1) if a fiber is subjected to a significant amount of bending, then the angle of incidence at the fiber wall can be reduced sufficiently for light to leave the core [37]; and (2) if two fibers pass close to one another and both have roughened surfaces, then light can pass between the fibers. Light coupling between adjacent fibers is a function of their separation [3].

An example of an optical fiber tactile sensor, whose sensing mechanism is based on the increase of light attenuation due to the microbend in the optical fibers, is shown in [Figure 25.11](#) [37]. The transducer consists of a four-layer, two-dimensional fiber optic array constructed by using two layers of optical fibers as a corrugation structure, through which microbends are induced in two orthogonal layers of active fibers. Each active fiber uses an LED as the emitter and a PIN photodiode as a detector. When an object is forced into contact with the transducer, a light distribution is detected at each detector. This light distribution is related to the applied force and the shape of the object. Using complex algorithms and active sensing (moving the object in relation to the transducer), the object position, orientation, size, and contour information can be retrieved [37]. However, the recovery of the applied force profiles was not reported in [37].

Photoelastic

An emerging technology in optical tactile sensing is the development of photoelastic transducers. When a light ray propagates into an optically anisotropic medium, it splits into two rays that are linearly polarized at right angles to each other and propagate at different velocities. This splitting of a ray into two rays that have mutually perpendicular polarizations results from a physical property of crystalline material that is called *optical birefringence* or simply *birefringence*. The direction in which light propagates with the higher velocity is called the *fast axis*; and the one in which it propagates more slowly is called the *slow axis*. Some optically isotropic materials — such as glass, celluloid, bakelite, and transparent plastics in general — become birefringent when they are subjected to a stress field. The birefringent effect lasts only during the application of loads. Thus, this phenomenon is called *temporary* or *artificial birefringence* or, more commonly, the *photoelastic phenomenon*.

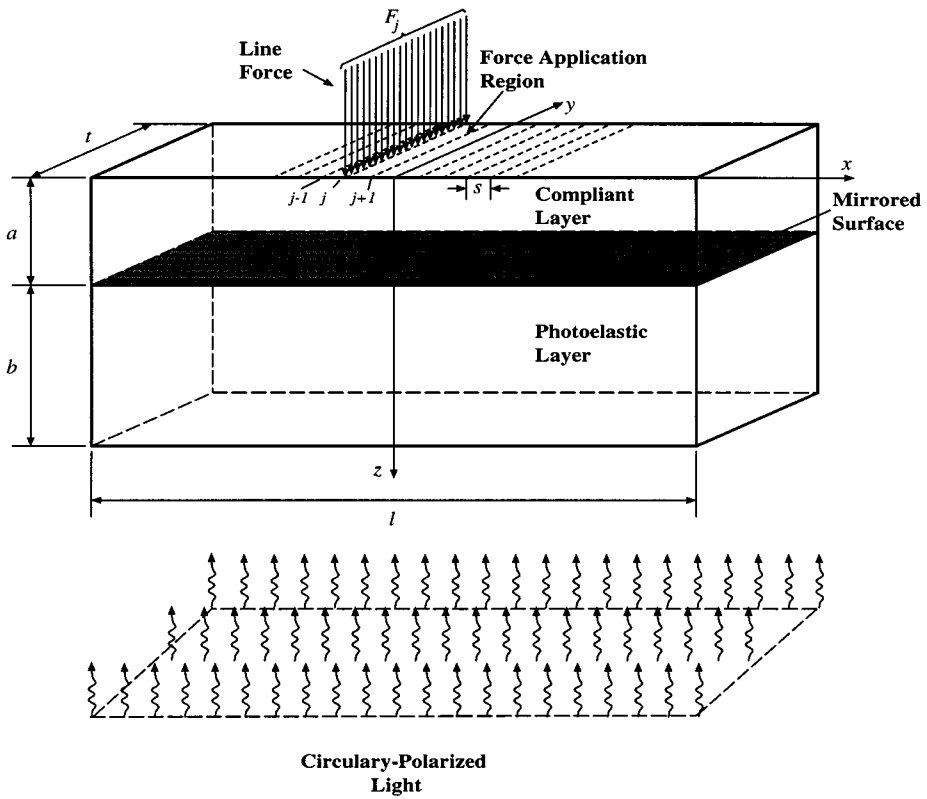
Figure 25.12(a) shows a photoelastic transducer proposed in [38]. It consists of a fully supported two-layer beam with a mirrored surface sandwiched in between. Normal line forces are applied to the top surface of the beam at discrete tactels, separated by equal distances, s , along the beam. The upper compliant layer is for the protection of the mirror, while the lower one is the photoelastic layer.

Circularly polarized monochromatic light, incident along the z -axis, illuminates the bottom surface of the transducer. The light propagates parallel to the z -axis, passes through the photoelastic layer, and then reflects back from the mirror. If no force is applied to the transducer, the returning light is circularly polarized because unstressed photoelastic material is isotropic. If force is applied, stresses are induced in the photoelastic layer, making the material birefringent. This introduces a certain phase difference between the components of the electric field associated with the light-wave propagation. The two directions of polarization are in the plane perpendicular to the direction of propagation (in this case, the x - y plane). As a consequence of this effect, the output light is elliptically polarized, creating a phase difference distribution, p , between the input light and the output light at each point in the x - y plane. The phase difference distribution carries the information of the force distribution applied to the transducer.

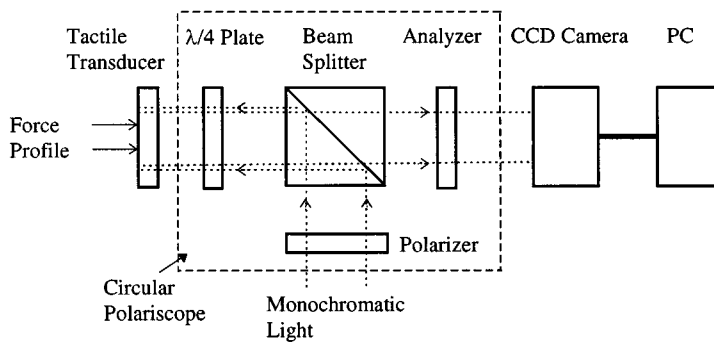
A *polariscope* is a practical method to observe the spatial variation on light intensity (fringes) due to the effect of induced phase difference distribution. Polariscopes can be either linear or circular, depending on the required polarization of the light. They can also be characterized as a reflective or a transparent type, depending on whether the photoelastic transducer reflect or transmits the light.

A circular, reflective polariscope, shown in Figure 25.12(b), is utilized to illuminate the transducer shown in Figure 25.12(a). The input light is linearly polarized and is directed toward the photoelastic transducer by a beam splitter. Before reaching the transducer, the light is circularly polarized by a quarter-wave plate. The output light is elliptically polarized when a force is applied. This light is directed toward a detector passing through the quarter-wave plate, the beam splitter, and an analyzer. Finally, it is detected by a camera linked to a frame grabber connected to a PC, for further data processing. The light that illuminates the camera consists of a set of fringes from where the force distribution applied to the transducer must be recovered. A technique for the recovery of the forces from the fringes is described in [38]. A model of the transducer using FEA is reported in [39].

One of the earlier applications of photoelasticity to tactile sensing dates back to the development phase of the Utah/MIT dexterous hand [40]. The researchers proposed the use of the photoelastic phenomenon as a transduction method for the recovery of the force profile applied to the fingers of the hand. They limited their application to the development of a single-touch transducer, although they claimed that an array of such devices could be implemented. However, the construction of a large array of their devices would be difficult. To overcome this difficulty, another research group proposed a different transducer [41]. Although an analytical model was developed for the sensor, a systematic method for recovering the two-dimensional force profile from the light intensity distribution was not reported. Thus, the sensor was used mainly for the study of the forward analysis, namely, observing the light intensity distribution for different touching objects brought into contact with the sensor. This sensor could eventually be used for determining some simple geometric properties of a touching object.



(a)



(b)

FIGURE 25.12 (a) Photoelastic transducer. (b) Circular reflective polariscope.

A tactile sensor reported in [42] is capable of detecting slippage. The output light intensity (the fringe pattern) is captured by a camera interfaced to a PC. When an object moves across the surface of the transducer, the light intensity distribution changes. A direct analysis of the fringes is used to detect movement of the grasped object; a special technique was reported to optimize the comparison process for detecting differences between two fringe patterns occurring due to the slippage of the object in contact with the sensor [42]. It is important to note that such an analysis of the fringes does not require the recovery of the applied force profile.

Photoelasticity offers several attractive properties for the development of tactile sensors: good linearity, compatibility with vision-base sensing technologies, and high spatial resolution associated with the latter, that could lead to the development of high-resolution tactile imagers needed for object recognition and fine manipulation. Also, photoelastic sensors are compatible with fiber optic technology that allows remote location of electronic processing devices and avoidance of interference problems.

Other technologies for tactile sensing include acoustic, magnetic, and microcavity vacuum sensors [43, 44].

References

1. P. Dario, Contact sensing for robot active touch, in *Robotic Science*, M. Brady (ed.), Cambridge, MA: MIT Press, 1989, chap. 3, 138-163.
2. P. P. L. Regtien, Tactile imaging, *Sensors and Actuators, A*, 31, 83-89, 1992.
3. R. A. Russell, *Robot Tactile Sensing*, Brunswick, Australia: Prentice-Hall, 1990.
4. A. D. Berger and P. K. Khosla, Using tactile data for real-time feedback, *Int. J. Robotics Res.*, 10(2), 88-102, 1991.
5. S. Begej, Planar and finger-shaped optical tactile sensors for robotic applications, *IEEE J. Robotics Automation*, 4, 472-484, 1988.
6. R. A. Russell and S. Parkinson, Sensing surface shape by touch, *IEEE Int. Conf. Robotics Automation*, Atlanta, GA, 1993, 423-428.
7. R. D. Howe, A tactile stress rate sensor for perception of fine surface features, *IEEE Int. Conf. Solid-State Sensors Actuators*, San Francisco, CA, 1991, 864-867.
8. S. Sugiyama, K. Kawahata, H. Funabashi, M. Takigawa, and I. Igarashi, A 32×32 (1K)-element silicon pressure-sensor array with CMOS processing circuits, *Electron. Commun. Japan*, 75(1), 64-76, 1992.
9. J. S. Son, E. A. Monteverde, and R. D. Howe, A tactile sensor for localizing transient events in manipulation, *IEEE Int. Conf. Robotics Automation*, San Diego, CA, 1994, 471-476.
10. M. R. Tremblay and M. R. Cutkosky, Estimating friction using incipient slip sensing during manipulation task, *IEEE Int. Conf. Robotics Automation*, Atlanta, GA, 1993, 429-434.
11. S. Omata and Y. Terubuna, New tactile sensor like the human hand and its applications, *Sensors and Actuators, A*, 35, 9-15, 1992.
12. R. Bayrleithner and K. Komoriya, Static friction coefficient determination by force sensing and its applications, *IROS'94*, Munich, Germany, 1994, 1639-1646.
13. M. A. Abidi and R. C. Gonzales, The use of multisensor data for robotic applications, *IEEE Trans. Robotics Automation*, 6, 159-177, 1990.
14. A. A. Cole, P. Hsu, and S. S. Sastry, Dynamic control of sliding by robot hands for regrasping, *IEEE Trans. Robotics Automation*, 8, 42-52, 1992.
15. P. K. Allen and P. Michelman, Acquisition and interpretation of 3-D sensor data from touch, *IEEE Trans. Robotics Automation*, 6, 397-404, 1990.
16. H. R. Nicholls (ed.), *Advanced Tactile Sensing for Robotics*, Singapore: World Scientific Publishing, 1992.

17. J. G. Webster (ed.), *Tactile Sensors for Robotics and Medicine*, New York: John Wiley & Sons, 1988.
18. R. S. Fearing, Tactile sensing mechanism, *Int. J. Robotics Res.*, 9(3), 3-23, 1990.
19. T. H. Speeter, Three-dimensional finite element analysis of elastic continua for tactile sensing, *Int. J. Robotics Res.*, 11(1), 1-19, 1992.
20. Y. C. Pati, P. S. Krishnaprasad, and M. C. Peckerar, An analog neural network solution to the inverse problem of early taction, *IEEE Trans. Robotics Automation*, 8(2), 196-212, 1992.
21. L. D. Harmon, Automated tactile sensing, *Int. J. Robotics Res.*, 1(2), 3-32, 1982.
22. W. E. Snyder and J. St. Clair, Conductive elastomers as a sensor for industrial parts handling equipment, *IEEE Trans. Instrum. Meas.*, 27(1), 94-99, 1991.
23. M. Shimojo, M. Ishikawa, and K. Kanaya, A flexible high resolution tactile imager with video signal output, *IEEE Int. Conf. Robotics Automation*, Sacramento, CA, 1991, 384-391
24. W. D. Hillis, A high resolution imaging touch sensor, *Int. J. Robotic Res.*, 1(2), 33-44, 1982.
25. Y. Yamada and M. R. Cutkosky, Tactile sensor with 3-axis force and vibration sensing functions and its applications to detect rotational slip, *IEEE Int. Conf. Robotics Automation*, San Diego, CA, 1994, 3550-3557.
26. K. Njafi and C. H. Mastrangelo, Solid-state microsensors and smart structure, *Ultrasonic Symp.*, Baltimore, MD, 1993, 341-350.
27. F. Zhu and J. W. Spronck, A capacitive tactile sensor for shear and normal force measurements, *Sensors and Actuators, A*, 31, 115-120, 1992.
28. K. Suzuki, K. Najafi, and K. D. Wise, A 1024-element high-performance silicon tactile imager, *IEEE Trans. Electron Devices*, 17(8), 1852-1860, 1990.
29. M. R. Wolfenbuttel and P. L. Regtien, The accurate measurement of a micromechanical force using force-sensitive capacitances, *Conf. Precision Electromagnetic Meas.*, Boulder, CO, 1994, 180-181.
30. M. R. Wolfenbuttel, R. F. Wolfenbuttel, and P. P. L. Regtien, An integrated charge amplifier for a smart tactile sensor, *Sensors and Actuators, A*, 31, 101-109, 1992.
31. E. D. Kolesar, Jr. and C. S. Dyson, Object imaging with piezoelectric robotic tactile sensor, *J. Microelectromechanical Syst.*, 4(2), 87-96, 1995.
32. J. L. Scheiter and T. B. Sheridan, An optical tactile sensor for manipulators, *J. Robot Computer-Integrated Manufacturing*, 1, 65-71, 1989.
33. R. Ristic, B. Benhabib, and A. A. Goldenberg, Analysis and design of a modular electrooptical tactile sensor, *IEEE Trans. Robotics Automation*, 5(3), 362-368, 1989.
34. H. Maekawa, K. K. Tanie, K. Komoriya, M. Kaneko, C. Horiguchi, and T. Sugawara, development of a finger shaped tactile sensor and it evaluation by active touch, *IEEE Int. Conf. Robotics Automation*, Nice, France, 1992, 1327-1334.
35. M. Ohka, Y. Mitsurya, S. Takeuchi, and O. Kamekawa, A three-axis optical tactile sensor (fem contact analyses and sensing experiments using a large-sized tactile sensor), *IEEE Int. Conf. Robotics Automation*, Nagoya, Aichi, Japan, 1995, 817-824.
36. J. Rebman and K. A. Morris, A tactile sensor with electro-optical transduction, in *Robots Sensors, Tactile and Non-Vision*, Vol. 2, A. Pugh (ed.), EFS Publications, 1986, 145-155.
37. S. R. Emge and C. L. Chen, Two dimensional contour imaging with a fiber optic microbend tactile sensor array, *Sensors and Actuators, B*, 3, 31-42, 1991.
38. R. E. Saad, A. Bonen, K. C. Smith, and B. Benhabib, Distributed-force recovery for a planar photoelastic tactile sensor, *IEEE Trans. Instrum. Meas.*, 45, 541-546, 1996.
39. R. E. Saad, A. Bonen, K. C. Smith, and B. Benhabib, Finite-element analysis for photoelastic tactile sensors, *Proc. IEEE Int. Conf. Industrial Electronics, Control, and Instrumentation*, Orlando, FL, 1995, 1202-1207.
40. S. C. Jacobsen, J. E. Wood, D. F. Knutti, and B. Biggers, The Utah/MIT dexterous hand: work in progress, in *Robotics Research: The First International Symposium*, M. Brady and R. Paul (eds.), Cambridge: MIT Press, 1983, 601-653.
41. A. Cameron, R. Daniel, and H. Durrant-Whyte, Touch and motion, *IEEE, Int. Conf. Robotics Automation*, Philadelphia, PA, 1988, 1062-1067.

42. S. H. Hopkins, F. Eghtedari, and D. T. Pham, Algorithms for processing data from a photoelastic slip sensor, *Mechatronics*, 2(1), 15-28, 1992.
43. S. Ando and H. Shinoda, Ultrasonic emission tactile sensing, *IEEE Trans. Control Syst.*, 15(1), 61-69, 1996.
44. J. C. Jiang, V. Faynberg, and R. C. White, Fabrication of micromachined silicon tip transducer for tactile sensing, *J. Vacuum Sci. Technol., B*, 11, 1962-1967, 1993.